Case Studies in Thermal Engineering 27 (2021) 101227

Contents lists available at ScienceDirect

Case Studies in Thermal Engineering

journal homepage: www.elsevier.com/locate/csite

Insight into the dynamics of time-dependent cross nanofluid on a melting surface subject to cubic autocatalysis

Syed Zahir Hussain Shah [a], Assad Ayub [a], Zulqurnain Sabir [a], Waleed Adel [b], Nehad Ali Shah [c], Se-Jin Yook [d,*]

[a] Department of Mathematics & Statistics, Hazara University, Mansehra, 21300, Pakistan
[b] Department of Mathematics and Engineering Physics, Faculty of Engineering, Mansoura University, Egypt
[c] Department of Mathematics, Lahore Leads University, Lahore, Pakistan
[d] School of Mechanical Engineering, Hanyang University, 222 Wangsimni-ro, Seongdong-gu, Seoul, 04763, Republic of Korea

ARTICLE INFO

Keywords:
Nanoparticle of iron oxide
Cross nanofluid model
Homogeneous-heterogeneous chemical process
bvp4c
Keller-box techniques

ABSTRACT

Current work unfolds the transport of energy of blood containing nanoparticles of iron oxide (Fe_3O_4) and mass transport is focalized by considering the homogeneous-heterogeneous chemical process with attached mathematical model of Cross nanofluid. The chemical process is carried out by chemical species and autocatalysis. Nonlinear Partial differential equations (PDEs) are appeared by mathematical model of Cross nanofluid and further delt with transformation for conversion of PDEs into Ordinary differential equations (ODEs). Purpose of numerical outcome of this study is analyzed by two schemes named as two schemes i.e., bvp4c and KELLER-BOX. Comparison of these schemes are investigated through tabular data and statistical bar graphs. From conclusion it is noticed that mass transport is increased with greater homogeneous-heterogeneous chemical parameter. Nanoparticles in fluid boosts the heat transfer. Melting process increase the transport of heat and skin friction. Both schemes are compared and found smooth agreements.

1. Introduction

Transmission of energy through convection mode is to make transport of heat from one place to another place due to movement of layers of fluid. In convection each individual particle takes the part for this transmission. In fluid, actually convection mode of energy transfer is taken place with process of heat diffusion (conduction) and heat transfer by bulk flow (advection) or macroscopic motion. This motion contains a fact that, at any moment infinite number of molecules are moving collectively or as aggregates. This type of motion during the temperature gradient makes transport of energy. In liquids and gases, the Convection mode keeps its dominant role during transport of energy. Thermal expansion of fluid layers also force convection while, in other cases when fluid is heated up then only natural buoyancy forces are responsible for motion in fluid so, this process is called natural convection. Convective heat transport has many applications in bio and nano heat transport. In other engineering field its applications are Thermal optimization, Cooling/heating system design Electric fan simulation, Heat sink simulation and Heat removal Heat sensitivity studies etc. Several scholars [1–6] made their investigations related to convective heat transport with mathematical model of different fluidic models like Carreau,

* Corresponding author.
E-mail addresses: zahirkazmi5@gmail.com (S.Z. Hussain Shah), assadayub610@gmail.com (A. Ayub), zulqurnain_maths@hu.edu.pk (Z. Sabir), waleedadel85@gmail.com (W. Adel), nehadali199@yahoo.com (N.A. Shah), ysjnuri@hanyang.ac.kr (S.-J. Yook).

https://doi.org/10.1016/j.csite.2021.101227
Received 8 June 2021; Received in revised form 3 July 2021; Accepted 4 July 2021
Available online 14 July 2021

Nomenclature

V, τ	Velocity, Cauchy tensor
u_{xx}, $f_{\eta\eta}$	Second derivative of f, u
f_{η}, u_x	Single derivative of f, u
$(T_1)_x$, $(Gb)_x$, $(Ga)_x$	Single derivative of (T_1), (Gb), (Ga)
$(T_1)_{xx}$, $(Gb)_{xx}$, $(Ga)_{xx}$	Second derivative of (T_1), (Gb), (Ga)
$(T_1)_x$, $(Gb)_x$, $(Ga)_x$	Single derivative of (T_1), (Gb), (Ga)
p, I, A_1	Pressure, identity tensor, Rivilin tensor
μ_∞, μ_0	lower shear rate and higher shear rate viscosity
$A = \frac{a}{c}$	Unsteady parameter
$\lambda = \frac{g\beta_f(T_2-T_m)}{u_w{}^2}$	Convection parameter
$M = \frac{(C_p)_f(T_2-T_m)x}{\lambda^*+c_s(T_m-T_0)}$	Melting parameter
$\mathrm{Pr} = \frac{(\rho C_p)_f}{\mu_{nf}}$	Prandtl number
$\mathrm{Re}_x = \frac{(u_w)}{\upsilon_f}$	Reynold number
$\beta_{nf}\left(\frac{1}{K}\right)$	Coefficient of thermal expansion
$k_{nf}\left(\frac{W}{Km}\right)$	Effective thermal conductivity
$\rho_f\left(\frac{kg}{m^3}\right)$	Reference density of fluid
$\rho_s\left(\frac{kg}{m^3}\right)$	Reference density of solid
$\mu_f\left(\frac{Ns}{m^2}\right)$	Viscosity of fluid
$\lambda^*\left(\frac{J}{kg}\right)$	Latent heat transfer of fluid
$c_s\left(\frac{J}{K}\right)$	Heat capacity of solid surface
We	Weissenberg number
$u(m/s)$	Velocity along x axis
$v(m/s)$	Velocity along y axis
$T_1(K)$	Temperature of nanofluid
$\varepsilon_1 = \sqrt{2\left(\frac{\upsilon}{b(m+1)}\right)x^{1-m}k_s}$	Diffusion coefficient
$T_2(K)$	Temperature of ambient fluid
$\rho_{nf}\left(\frac{kg}{m^3}\right)$	Density of nanofluid
$\mu_{nf}\left(\frac{Ns}{m^2}\right)$	Effective viscosity of nanofluid
$g(m/s^2)$	Gravitational acceleration
φ	volume fraction of nanofluid
$k_f(W/Km)$	Thermal conductivity of fluid
$k_s(W/Km)$	Thermal conductivity of solid
a, c	Constant
n	Cross fluid index
k2	homogeneous reaction parameter

Maxwell, Casson nanofluid. Mixed convective flow of blood with considering nano particles of copper along inclined geometry is explained by Umadevi et al. [7].

Moradi et al. [8] described a comprehensive note on experimental water nanofluids flow and heat transfer in double-pipe heat exchanger. MHD Bingham fluid due to peristalsis with multiple chemical reactions along aspect of application to blood flow with geometry of through narrow arteries is brought by Vaidya et al. [9]. Assisting/opposing buoyancy effect on different mathematical model with orthogonal magnetic effect, nonlinear thermal radiation and multiple features is examined by Chamkha et al. [10]. Abbas et al. [11] did research on convective transport in aluminum tube with considering the water as a based fluid. Checkup related to wall properties and convective heat transfer with geometry of isothermal channel is pointed out by Yao et al. [12].

Evaluation related to dynamic viscosity and energy transport of hybrid nanofluid with engine oil as a lubricant is investigated by Goodarzi et al. [13]. Furthermore, studies related to development of ANNs with attached suitable architectures and training algorithms along support of sensitivity analysis, MHD mixed convection transport of heat and discussion about entropy generation in a lid-driven cavity with geometry of rotating cylinders fetched by Refs. [14,15].

Nanofluid is the class of nanotechnology that is based on heat transfer fluid. Nanofluid is obtained by stably suspending and dispersing nanoparticle in conventional fluid with dimension of order 100 nm. First time the term nanofluid is exercised by choi [16] and on this base he described new class of nanotechnology with linkage of thermal properties. The goal of nanofluid is to achieve highest thermal performance at lower possible concentration. Nanofluid maximizes the thermal conductivity. Nanoparticles are made of metal, carbides and carbon nanotubes etc. Nanofluid like fog, small dust are being utilized in solar energy, warmth exchanger, automobile heaters and electrical chips etc. Blood flow of nanofluid through an artery with composite stenosis and permeable walls is described by Ellahi et al. [17]. Rashidi et al. [18] depicted entropy generation on MHD blood flow of nanofluid due to peristaltic waves. Chahregh et al. [19] publishes his work about TiO_2–Ag/blood hybrid nanofluid flow through an artery with applications of drug delivery and blood circulation in the respiratory system. Computational simulations of hybrid mediated nano-hemodynamics (Ag–Au/Blood) through an irregular symmetric stenosis is explored by Tripathi et al. [20]. Toghraie et al. [21] presented the analysis on water/CuO nanofluid with geometry of L-shaped porous ribs microchannels.

Applying the force on fluid, this force brings change in shape or structure of fluid that is called deformation. Relation between applied force and deformation is linear then fluid is Newtonian otherwise fluid goes in category of non-Newtonian like toothpaste, ketchup, paint, blood and starch etc. To explore properties of these non-Newtonian fluids many mathematical models are there like Carreau, Casson, Maxwell, Williamson and power law model etc. but these models are failed to investigate the properties of fluid at very high and low shear rate. To depict the properties of any fluid at very higher shear rate and very lower shear rate Cross fluid model was exercised by Cross [22]. This model has super capability to overcome the problem that is faced when shear rate is largely increased or decreased. Many researchers [23,24] are working in this model for blood and its unique properties. Nazeer et al. [25] described the heat transport via heat sink source and radiation on cross fluid and found that velocity of fluid is interlinked with radiation parameter. Impact of inclined magnetic field on velocity of Cross fluid, radiation impact of temperature, activation energy on concentration of cross fluid is described by several interpreters Sabir et al. [26]. Orthogonal magnetic dipole effect on Cross fluid with multiple features is explored by Yao et al. [27]. Activation energy and thermophoretic effect on Cross fluid is depicted by khan et al. [28]. Higher order process of chemical reaction and Lorentz force effect on Cross fluid is interpreted by Sharma et al. [29]. Here in this study, it is found that Lorentz force reduces the velocity of micropolar fluid and chemical reaction improves the concentration of said fluid.

Chemical reactions are vital part of our daily life and has applications as polymer production, ceramics, dispersion and fog formation, food processing and hydrometallurgical industry. Uncountable life supported activities are taken place through chemical reactions, and we can say that revolutionary set up has been marked with composing different items to obtain best products. Several systems related to chemical reacting species based upon homogeneous-heterogeneous chemical reactions like biochemical frameworks, catalysis and burning etc. Perplexed association exists among different features of homogeneous and heterogeneous reactions. Segment of chemical reaction has capacity to continue gradually not at all except in the catalyst existence. Several scholars utilized homogeneous-heterogeneous chemical reactions to investigate the flow attitude of many fluidic models [30–35]. Toghraie et al. [36] investigated Blood flow analysis inside different arteries Sisko model with chemical reactions. Ijaz et al. [37] depicted about entropy analysis in nonlinearly convective flow of the Sisko model with considering the impact of Joule heating and chemical reaction. A novel data envelopment analysis cross-model integrating interpretative structural model and energy efficiency evaluation with chemical reaction is made by Han et al. [38]. Zyphur et al. [39] upgraded building a general cross-lagged panel model with different approach. Gheynani et al. [40] made study related of nanoparticles diameter on turbulent flow and heat transfer properties with microtube. Optimal arrangements of a heat sink on hybrid nanofluid is clearly defined by Ref. [41].

Basic intend of this study is to unfold the Mass transport of blood through chemical species with time dependent Cross nanofluid. Emerged PDEs are governed with similarity transformation and further these are transformed into ODEs. These ODEs are tackled by BVP4C and KELLER-BOX technique for numerical solution and comparison between both techniques is also made.

Remaining part of paper has the sections of Physical model, validity of study, analytical and solver MATLAB methodology, KELLER-BOX technique, result and discussion and main outcomes of this work.

2. Origination of equation of cross fluid model

Equations for problem (write in del form)

$$u_x + v_x = 0 \tag{1}$$

$$\begin{aligned} &uu_x + vu_y + u_t = \nu\left[\left(\left(\Gamma u_y\right)^n + 1\right)^{-1}\right]u_{yy} \\ &-\left(u_y\right)^n u_{yy}\left[1 + \left(\Gamma u_y\right)^n\right]^{-2}\nu\Gamma^n n + g\beta_{nf}\left(T_1 - T_2\right) \end{aligned} \tag{2}$$

Table 1
Description of basic quantities.

Characteristics of fluid	Standard units	Characteristics of Iron oxide (Fe3O4)	Characteristics of Blood
Density of fluid	$(kg)m^{-3}$	5.180×10^{3}	1.050×10^{3}
(Thermal conductivity) or thermal conductance	$W(K \cdot m)^{-1}$	0.0970×10^{2}	5.20×10^{-1}
Coefficient related to thermal expansion	$1/K$	0.013×10^{-3}	1.8×10^{-4}
Capacitance of energy/heat	JK^{-1}	0.0670×10^{4}	3.617×10^{-3}

Table 2
Computing the Comparison with existed previous work for $-\theta'(0)$. $A = \varphi = \mathrm{We} = \lambda = 0 = \mathrm{Sc}$

Pr	Ref [43]	Ref [44]	Ref [45]	Present bvp4c	Present Keller-box Scheme
0.72	1.08	1.088	1.08231	1.08240223255	1.082402456823
1.00	1.33	1.333	1.33372	1.333687691234	1.333687612342
10.00	4.79	4.796	4.79673	4.796812643246	4.796816714125

$$v(T_1)_x + u(T_1)_x + (T_1)_t = \alpha_{nf}(T_1)_{yy} \tag{3}$$

3. Geometry related physical model

Two dimensional, Incompressible and time dependent flow of Cross fluid that is blood is here by supposed. In considered fluid (blood), nanoparticles of iron oxides (Fe3O4) are flowing along a vertical surface are incorporated. It is made assumption that flow goes towards x-axis, and y-axis is clearly perpendicular to x-axis and presented by geometrical Fig. 1. Energy transport of blood is countered through melting heat phenomenon and relocation of mass is judged through chemical species with heterogeneous/homogeneous reactions. Let now P and Q are two autocatalysts in case of isothermal reaction.

$$P + 2Q \rightarrow 3Q, \text{ and rate } R = k_1 G_a G_b{}^2 \tag{4}$$

In case of single order, it goes as

$$P \rightarrow Q, \text{ and rate } R = k_s G_a \tag{5}$$

Away from the field the $rate = k_s G_a G_b{}^2$ becomes $rate = k_s G_a G_b{}^2 = 0$, k_s, k_1, is rate coefficient of heterogeneous/homogeneous reactions, G_a, G_b is concentration of chemical specie E, F respectively. Furthermore, Flow is kept bounded in 1st and 2nd quadrant that is in $y > 0$. T_m is assumed the temperature of surface and temperature of ambient medium is T_2. Thermophysical characteristics are unfolded by Table 1.

Using all the calculations through boundary layer analysis set of PDEs is taken the form as [42]:

$$u_x + v_x = 0 \tag{6}$$

$$\begin{aligned} &uu_x + vu_y + u_t = \nu\left[\left((\Gamma u_y)^n + 1\right)^{-1}\right]u_{yy} \\ &-(u_y)^n u_{yy}\left[1 + (\Gamma u_y)^n\right]^{-2}\nu\Gamma^n n + g\beta_{nf}(T_1 - T_2) \end{aligned} \tag{7}$$

$$v(T_1)_x + u(T_1)_x + (T_1)_t = \alpha_{nf}(T_1)_{yy} \tag{8}$$

$$u(G_a)_x + v(G_a)_y + (G_a)_t = \alpha_{nf}(G_a)_{yy} - k_1 G_a G_b{}^2, \tag{9}$$

$$u(G_b)_x + v(G_b)_y + (G_b)_t = \alpha_{nf}(G_b)_{yy} + k_1 G_a G_b{}^2, \tag{10}$$

Attached BCs are written below as:

$$\begin{aligned} &u = u_w(x,t), \text{ where } u_w(x,t) = ax(1-ct)^{-1}, \\ &T_1 = T_m, \ (G_b)_y = k_s G_b, \quad (G_a)_y = 0, \ at\ y = o \end{aligned} \tag{11}$$

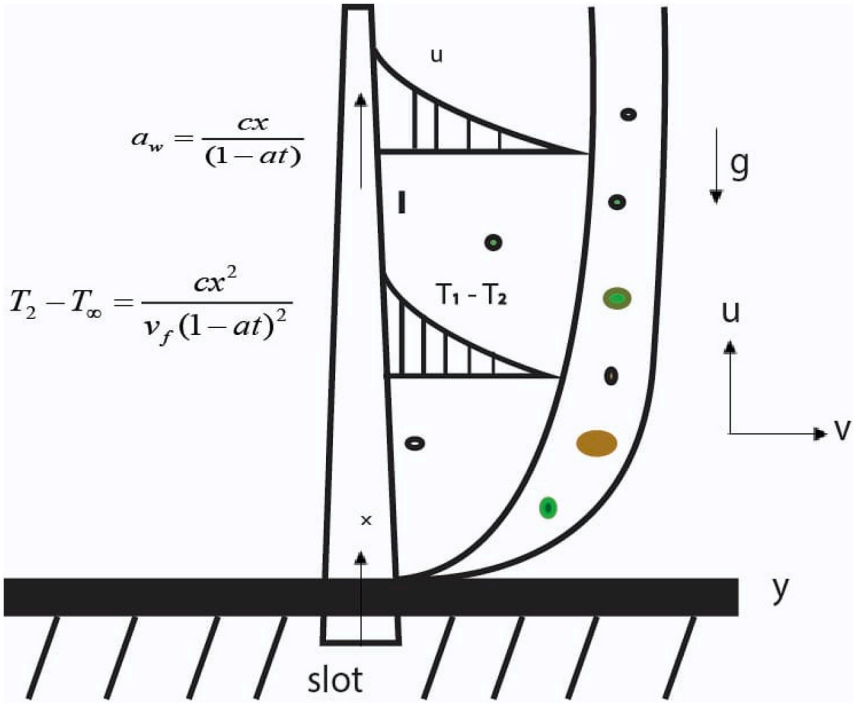

Fig. 1. Interpreter sketch of fluid.

$$\text{for } y \to \infty, (-)\{K_{nf}(T_1)_y\}_{y=0} = \langle \lambda^* - (T - T_{mo})c_s \rangle v(x,o)\rho_f \\ G_a \to 0,\ G_b \to 0 \tag{12}$$

Similarity transformation tool for Eqs (19-22)

$$\psi = \left(v_f\,(1-\alpha t)^{-1}c\right)^{1/2} f(\eta)x, \quad \frac{\eta}{y} = \sqrt{((1-\alpha t)^{-1}(v_f)^{-1}c)},\ u = \psi_y = \left(\frac{(1-\alpha t)^{-1}c}{x^{-1}}\right)f'(\eta), \\ v = -\psi_x = ag'(\eta)y,\ \theta(\eta) = \left[(T_2 - T_m)^{-1}(T_1 - T_2)\right],\ G_a = G_\infty \phi(\eta),\ G_b = G_\infty \vartheta(\eta), \tag{13}$$

$$\frac{\mu_{nf}}{\mu_f} = \left[(1-\varphi)^{2.5}\right],\ \alpha_{nf} = \left[\left(\rho C_p\right)_{nf}\right]^{-1} k_{nf} = \frac{1}{(1-\varphi)^{-1}}\left(\rho C_p\right)_f + \varphi\left(\rho C_p\right)_s, \quad \rho_{nf} = (1-\varphi)\rho_f + \varphi(\rho)_s. \\ \frac{k_{nf}}{k_f} = \left[\frac{X}{Y}\right];\ X = \left(2k_s + k_f\right) - 2\left(k_f - 2k_s\right)\varphi,\ Y = \left(2k_s + k_f\right) + \left(k_f - 2k_s\right)\varphi,\ \beta_{nf} = (1-\varphi)\beta_f + \varphi\beta_s \tag{14}$$

Using Eqs (19-22), the updated form is given as:

$$A\left[H + \frac{\eta}{2}f''\right](1 + (wef'')^n)^2 = \left[\left\{\left(1-\varphi\right) + \varphi\frac{\rho_s}{\rho_f}\right\}\left\{(1-\varphi)^{2.5}\right\}\right]^{-1}\left[(1 - (n-1)(wef'')^n)\right]f''' \\ + \left\{\left(1-\varphi\right) + \varphi\frac{\beta_s}{\beta_f}\right\}\lambda\theta - f_\eta^{\,2} - f_{\eta\,\eta} \tag{15}$$

$$\theta_{\eta\eta} - \Pr\left(k_{nf}\right)^{-1} k_f \left\{\left(1-\varphi\right) + \varphi\frac{\left(\rho C_p\right)_s}{\left(\rho C_p\right)_f}\right\}\left\{A\left(\frac{\eta\theta_\eta}{2} + 2\theta\right) - \theta_\eta f + 2\theta f_\eta\right\} = 0 \tag{16}$$

$$\phi_{\eta\eta} + Sc\frac{k_f}{k_{nf}}\left\{\left(1-\varphi\right) + \varphi\frac{\left(\rho C_p\right)_s}{\left(\rho C_p\right)_f}\right\}\left[A\left(\frac{\eta\theta_\eta}{2} + 2\theta\right) + F\phi + k_2\phi(1-\phi)^2\right] + \theta_{\eta\eta} = 0 \tag{17}$$

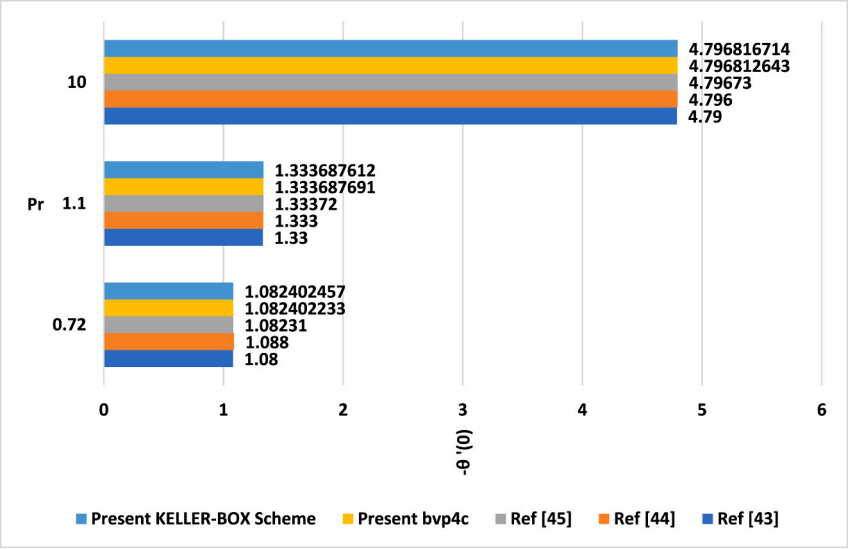

Fig. 1b. Graphical validity of study.

$$\vartheta_{\eta\eta} + Sc\frac{k_f}{k_{nf}}\left\{\left(1-\varphi\right)+\varphi\frac{\left(\rho C_p\right)_s}{\left(\rho C_p\right)_f}\right\}\left[A\left(\frac{\eta\theta_\eta}{2}+2\theta\right)+F\vartheta+k_2\vartheta(1-\vartheta)^2\right]+\theta_{\eta\eta}=0 \tag{18}$$

Transformed BCs for transformed ODEs

$$\begin{aligned} &M\theta_\eta(0)+\mathrm{Pr}f(0)=0,\ f_\eta=1,\ \phi_\eta(0)=0,\ \theta'=1,\ \vartheta'(0)=\varepsilon_1\vartheta(0),\ at\ \eta=0\\ &f_\eta\to 0,\quad \theta_\eta\to 0,\ \vartheta(\infty)\to 0,\phi(\infty)\to 0,\ at\ \eta=\infty \end{aligned} \tag{19}$$

Aspect of physical quantities

$$C_{fx}=2\tau_w\mu_{nf}\left(\rho_f u_w{}^2\right)^{-1}\left(u_y\right)_{y=o} \tag{20}$$

$$Nu_x=\left(T_1\right)_y\frac{k_{nf}(-x)(T_\infty-T_m)^{-1}x}{k_f}_{y=0} \tag{21}$$

Similarity variables fetch the bellow.

$$\frac{1}{2}Cf_x\left(\mathrm{Re}_x\right)^{0.5}(1-\varphi)^{2.5}[1+(We_1f''(0))^n]=f''(0) \tag{22}$$

$$Nu_x\sqrt{\left(\mathrm{Re}_x\right)^{-1}}=\left(k_{nf}/k_f\right)(-\theta'(0)) \tag{23}$$

4. Validness of study

Sanctioned Table 2 promotes to get latest calculation because this permits current attempt as agreement is found for $-\theta'(0)$ with existing literature Fig. 1b

5. Numerical procedure for solution and MATLAB methodology

The numerical procedures for the solutions are presented in the form of two ways, which are provided in detail as [46–55]:

$$f = W_1,$$

$$f_\eta = W_2, \quad f_{\eta\eta} = W_3,$$

$$f_{\eta\eta\eta} = W_3^{'}, \ \theta = W_4, \ \theta_\eta = W_5,$$

$$\theta_{\eta\eta} = W_6,$$

$$\phi = W_7, \ \phi_\eta = W_8, \ \phi_{\eta\eta} = W_9$$

$$\vartheta = W_{10}, \ \vartheta_\eta = W_{11}, \ \vartheta'' = W_{12}$$

$$W_3^{'} = \frac{A\left[W_2 + \frac{\eta}{2}W_3\right]}{\Omega_1 \times \Omega_2} - \left\{\left(1-\varphi\right) + \varphi\frac{\beta_s}{\beta_f}\right\}\lambda W_4 + {W_2}^2 + W \times W_3$$

$$W_6 = \frac{k_f}{k_{nf}} - \Omega_3\left\{A\left(2W_4 + \frac{\eta W_5}{2}\right) + 2W_4W_2 - W_5W_1\right\}$$

$$where \quad \Omega_1 = \left[\left\{\left(1-\varphi\right) + \varphi\frac{\rho_s}{\rho_f}\right\}\left\{(1-\varphi)^{2.5}\right\}\right]^{-1}$$

$$\Omega_2 = \left[(1-(n-1)(we_1W_3)^n)(1+(we_1W_3)^n)^{-2}\right]$$

$$\Omega_3 = \left\{\left(1-\varphi\right) + \varphi\frac{\left(\rho C_p\right)_s}{\left(\rho C_p\right)_f}\right\}$$

$$W_9 = -Sc\frac{k_f}{k_{nf}}\left\{\left(1-\varphi\right) + \varphi\frac{\left(\rho C_p\right)_s}{\left(\rho C_p\right)_f}\right\}\left[A\left(\frac{\eta W_5}{2} + 2W_4\right) + FW_7 + k_2W_7(1-W_7)\right] - W_6$$

$$W_{12} = -Sc\frac{k_f}{k_{nf}}\left\{\left(1-\varphi\right) + \varphi\frac{\left(\rho C_p\right)_s}{\left(\rho C_p\right)_f}\right\}\left[A\left(\frac{\eta W_5}{2} + 2W_4\right) + FW_7 + k_2W_7(1-W_7)\right] - W_6$$

Appling the shooting technique, the BCs take the form as:

$$\left|\begin{array}{l} MW_5(0) + \mathrm{Pr}W_1 = 0 \\ \quad W_2 = 1, \ W_9(0) = 0 \\ W_5 = 1, \ W_{11}(0) = \varepsilon_1 W_7(0), \ at\ \eta = 0 \\ W_2 \to 0, \quad W_5 \to 0, \\ W_{10}(\infty) \to 0, W_7(\infty) \to 0, \ at\ \eta = \infty \end{array}\right| \tag{24}$$

5.1. Flow chart of MATLAB scheme

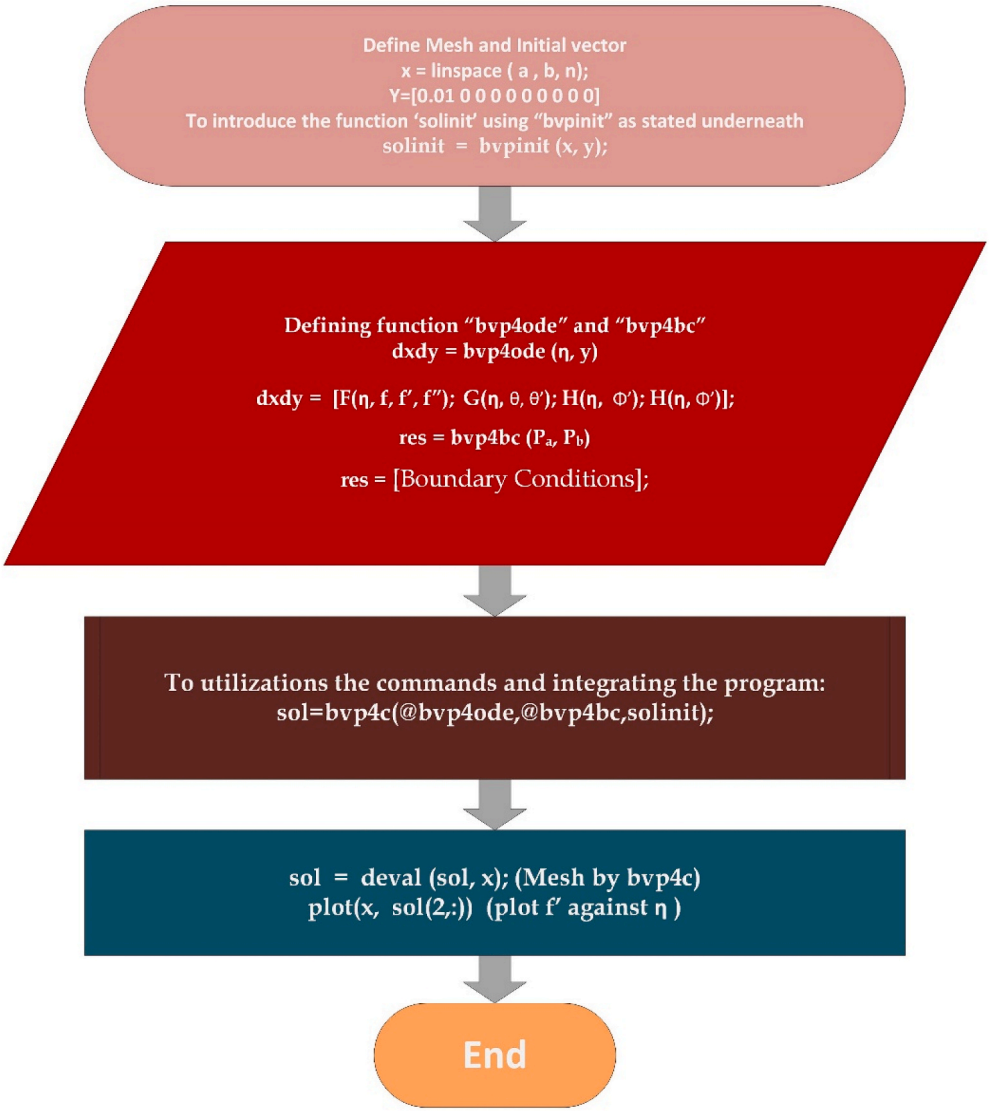

6. Procedure Keller–box method

The mentioned technique is most fast and convergent, works with three steps that are given as:

1. First, we convert higher-order differential Equations (ODEs) from 25 to 28 into first order ODEs.

$$f' = R,\ \theta' = S, \phi' = T,\ \vartheta' = U \tag{25}$$

Using in Eqs (25-28)

$$A\left[H + \frac{\eta}{2}R'\right](1 + (weR')^n)^2 = \left[\left\{\left(1-\varphi\right) + \varphi\frac{\rho_s}{\rho_f}\right\}\{(1-\varphi)^{2.5}\}\right]^{-1}[(1-(n-1)(weR')^n)]R'' + \left\{\left(1-\varphi\right) + \varphi\frac{\beta_s}{\beta_f}\right\}\lambda S - R'2 - R'f \tag{26}$$

$$S^{'}-\Pr\frac{k_f}{k_{nf}}\left\{\left(1-\varphi\right)+\varphi\frac{\left(\rho C_p\right)_s}{\left(\rho C_p\right)_f}\right\}\left\{A\left(\frac{\eta S}{2}+2\theta\right)-Sf+2\theta R\right\}=0 \tag{27}$$

$$T''+Sc\frac{k_f}{k_{nf}}\left\{\left(1-\varphi\right)+\varphi\frac{\left(\rho C_p\right)_s}{\left(\rho C_p\right)_f}\right\}\left[A\left(\frac{\eta S}{2}+2\theta\right)+F\phi+k_2\phi(1-\phi)\right]+S''=0 \tag{28}$$

$$U^{'}+Sc\frac{k_f}{k_{nf}}\left\{\left(1-\varphi\right)+\varphi\frac{\left(\rho C_p\right)_s}{\left(\rho C_p\right)_f}\right\}\left[A\left(\frac{\eta S}{2}+2\theta\right)+F\vartheta+k_2\vartheta(1-\vartheta)\right]+S^{'}=0 \tag{29}$$

The BCs take the form as:

$$\left|\begin{array}{l} MS(0)+\Pr f(0)=0 \\ \quad R=1,\ T(0)=0 \\ S=1,\ U(0)=\varepsilon_1\vartheta(0),\ at\ \eta=0 \\ R\to 0,\quad S\to 0, \\ \vartheta(\infty)\to 0,\phi(\infty)\to 0,\ at\ \eta=\infty \end{array}\right| \tag{30}$$

2. Formulation of grid points are needed to be set and described as

$$\eta_0=0,\ \eta_j=\eta_{j-1}+h_j,\ j=1,\ 2,\ 3,\ ...,\ J,\ \eta_J=\eta_\infty \tag{31}$$

Central difference approximations method is utilized to consider the arbitrary points

$$\frac{f_j-f_{j-1}}{h_j}=H_{j-\frac{1}{2}},\frac{\theta_j-\theta_{j-1}}{h_j}=L_{j-\frac{1}{2}},\ and\ f_{j-\frac{1}{2}}=\frac{f_j+f_{j-1}}{2}\ \frac{\phi_j-\phi_{j-1}}{h_j}=T\ \frac{\vartheta_j-\vartheta_{j-1}}{h_j}=U \tag{32}$$

$$\begin{aligned} &A\left[H_{j-\frac{1}{2}}+\frac{\eta}{2}\left(U_{j-\frac{1}{2}}\right)\right]\left(1+\left(we\left(H_{j-\frac{1}{2}}\right)\right)^n\right)^2=\left[\left\{\left(1-\varphi\right)+\varphi\frac{\rho_s}{\rho_f}\right\}\left\{(1-\varphi)^{2.5}\right\}\right]^{-1} \\ &*\left[\left(1-\left(n-1\right)\left(we\left(H_{j-\frac{1}{2}}\right)\right)^n\right)\right]\left[\frac{H_j-H_{j-1}}{h_j}\right]+\left\{\left(1-\varphi\right)+\varphi\frac{\beta_s}{\beta_f}\right\}\lambda l_{j-\frac{1}{2}}-\left(H_{j-\frac{1}{2}}\right)^2-H_{j-\frac{1}{2}}f_{j-\frac{1}{2}} \end{aligned} \tag{33}$$

$$\left[\frac{L_j-L_{j-1}}{h_j}\right]-\Pr\frac{k_f}{k_{nf}}\left\{\left(1-\varphi\right)+\varphi\frac{\left(\rho C_p\right)_s}{\left(\rho C_p\right)_f}\right\}\left\{A\left(\frac{\eta V_{j-\frac{1}{2}}}{2}+2\theta_{j-\frac{1}{2}}\right)-Lf+2\theta_{j-\frac{1}{2}}H_{j-\frac{1}{2}}\right\}=0 \tag{34}$$

$$T_{j-\frac{1}{2}}+Sc\frac{k_f}{k_{nf}}\left\{\left(1-\varphi\right)+\varphi\frac{\left(\rho C_p\right)_s}{\left(\rho C_p\right)_f}\right\}\left[A\left(\frac{\eta S}{2}+2\theta_{j-\frac{1}{2}}\right)+F\phi+k_2\phi(1-\phi)\right]+S_{j-\frac{1}{2}}=0 \tag{35}$$

$$T_{j-\frac{1}{2}}+Sc\frac{k_f}{k_{nf}}\left\{\left(1-\varphi\right)+\varphi\frac{\left(\rho C_p\right)_s}{\left(\rho C_p\right)_f}\right\}\left[A\left(\frac{\eta S}{2}+2\theta_{j-\frac{1}{2}}\right)+F\vartheta+k_2\vartheta(1-\vartheta)\right]+T_{j-\frac{1}{2}}=0 \tag{36}$$

3. **As system contains PDEs (40–43) is nonlinear so for further proceeding we use method of iteration so,** $(j+1)^{th}$iteration we make written as $f_{j+1}=f_j+\delta f_j$ and keep ignoring 2nd order for δf_j.

$$A\delta = r^*$$

$$A=\frac{\partial^2}{\partial x^2}\begin{bmatrix}[A_1] & [C_1] & & & & & \\ [B_2] & [A_2] & & [C_2] & & & \\ & & & \ddots & \ddots & & \\ & \ddots & \ddots & \ddots & & & \\ & & \ddots & & & & \\ & & & [B_{j-1}] & [C_{j-1}] & [C_{j-1}] & \\ & & & & [B_j] & [A_j] & \end{bmatrix},\ \delta=\begin{bmatrix}[\delta_1]\\ [\delta_2]\\ \ddots\\ \ddots\\ \ddots\\ \ddots\\ [\delta_{j-1}]\\ [\delta_j]\end{bmatrix},\ r^*=\begin{bmatrix}[r_1]\\ [r_2]\\ \ddots\\ \ddots\\ \ddots\\ \ddots\\ [r_{j-1}]\\ [r_j]\end{bmatrix}, \tag{37}$$

$$A=L^*U$$

$$L^*=\begin{bmatrix}[a_1] & & & \\ [b_2] & [a_2] & & \\ \ddots & \ddots & & \\ & \ddots & \ddots & \\ & & [b_j] & [a_j]\end{bmatrix},\ U=\begin{bmatrix}[I] & & [\Gamma_1] & & \\ & [I] & & [\Gamma_1] & \\ & & \ddots & & \ddots \\ & & [I] & [\Gamma_{J-1}] & \\ & & & & [I]\end{bmatrix} \tag{38}$$

Here unit matrix is $[I]$, the matrices $[ai]$ and $[\Gamma i]$ have 9×9 order and process of calculating its element as:

$$[a_i] = [A_i] \tag{39}$$

$$[A_1][\Gamma_1]=[C_1] \tag{40}$$

$$[a_j] = [A_j]-[B_j][\Gamma_{j-1}], j=1,2,3,\ldots,J \tag{41}$$

$$[a_i][\Gamma_1] = [C_j], j=1,\ 2,\ 3,\ \ldots,\ J \tag{42}$$

$$L^*U\delta = r^* \tag{43}$$

Assume that

$$U\delta = O \tag{44}$$

with

$$L^*O = r^* \tag{45}$$

Here

$$O=\begin{bmatrix}[O_1]\\ [O_2]\\ [O_3]\\ [O_4]\\ [O_5]\\ [O_6]\\ [O_7]\\ [O_8]\\ [O_9]\end{bmatrix} \tag{46}$$

where $[O_j]$ inculpates column matrices having 9×9 order, and computation process is given as:

Table 3
Description of skin friction with shear thinning/shear thickening case.

parameters			Skin friction			
A	We	ϕ	Shear thinning $n = -0.5$ with bvp4c/shooting	Shear thickening$n = 0.5$ with bvp4c/shooting	Shear thinning $n = -0.5$Keller box approach	Shear thickening $n = 0.5$Keller box approach
1.0	0.0	0.00	1.265627	0.5567	1.265627	0.5567
2.0	–	–	1.272716	0.41207	1.272716	0.41207
3.0	–	–	1.254575	0.45307	1.254575	0.45307
4.0	–	–	1.253714	0.47513	1.253714	0.47513
–	0.5	–	1.257613	0.45068	1.257613	0.45068
–	0.8	–	1.217261	0.45608	1.217261	0.45608
–	0.9	–	1.216731	0.34662	1.216731	0.34662
–	1.2	–	1.301221	0.37484	1.301221	0.37484
–	–	0.01	1.344344	0.39728	1.344344	0.39728
–	–	0.03	0.417206	0.45108	0.417206	0.45108
–	–	0.06	0.582658	0.46569	0.582658	0.46569

Table 4
Study of skin friction for assisting and opposing buoyancy force.

Parameters			Skin friction			
A	We	ϕ	Opposing flow$\lambda = -0.5$ with bvp4c/ shooting	Assisting flow $\lambda = 0.5$with bvp4c/ shooting	Opposing flow $\lambda = -0.5$ Keller box approach	Assisting flow $\lambda = 0.5$Keller box approach
1.0	0.0	0.00	1.24554	0.31561	1.24556	0.31581
2.0	–	–	1.34556	0.31345	1.34557	0.31395
3.0	–	–	1.23551	0.31836	1.23558	0.31866
4.0	–	–	1.24661	0.22332	1.24663	0.22382
–	0.5	–	1.29436	0.33687	1.29435	0.33687
–	0.8	–	1.34540	0.37123	1.34503	0.37133
–	0.9	–	1.33643	0.34342	1.33642	0.34362
–	1.2	–	1.37644	0.33823	1.37645	0.33873
–	–	0.01	1.37783	0.33789	1.37786	0.33739
–	–	0.03	0.52836	0.31857	0.52838	0.31817
–	–	0.06	0.61735	0.38593	0.61733	0.38593

Table 5
Physical quantities in respect of presence and absence of melting effect.

				$C_f\sqrt{(\mathrm{Re}_x)}$		$Nu_x\sqrt{(\mathrm{Re}_x)}$	
φ	λ	A	Pr	*Absence of M*	*Presence of M* $[M = 0.5]$	*Absence of M*	*Presence of M* $[M = 0.5]$
0.05	0.1	0.2	0.72	0.8645854	0.82761376	5.7635461	6.9450734567
0.07				0.5475461	0.85347681	6.8627223	7.9587504503
0.09				4.4087632	0.99431563	8.6546279	7.9942087676
	0.0			0.8242163	0.9654430	4.4756813	7.9345513231
	1.0			4.8854189	0.4145968	0.5450426	8.4534082323
	2.0			4.9635714	0.1865583	0.4243598	9.8897648674
		1.0		0.7823445	0.1878547	5.0126755	5.5082424239
		3.0		0.8987616	0.4596474	6.7125556	6.4359242348
		5.0		0.9276544	0.4897654	7.3354267	7.4776225674
			7.20	0.71236191	0.9832787	5.4027687	7.464550832
			14.4	0.73234567	0.9985332	6.3324910	9.4347855045
			21.6	7.8912127	0.9999668	7.23465478	11.456104567

$$[a_1][O_j] = [r_1] \tag{47}$$

$$[a_j][O_j] = [r_j] - [B_j][O_{j-1}] \tag{48}$$

After getting the results of P, δ elements, the calculated form becomes as:

$$[\delta_j] = [O_j] \tag{49}$$

$$[\delta_j] = [O_j] - [\Gamma_j][\delta_{j+1}] \tag{50}$$

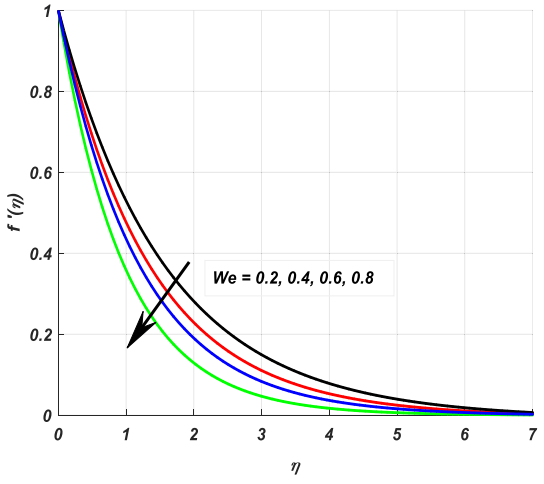

(a): Velocity attached with *We*.

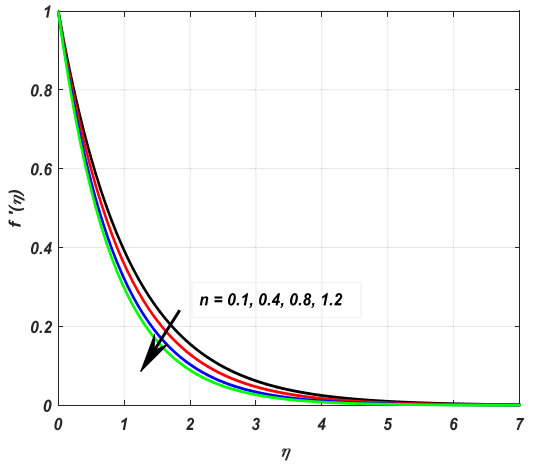

(b): Velocity attached with *n*.

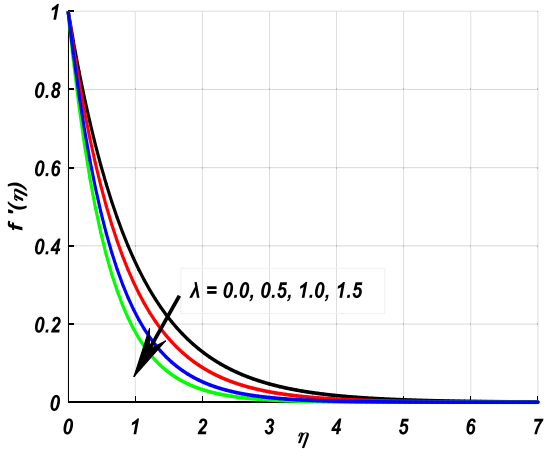

(c): Velocity attached with λ.

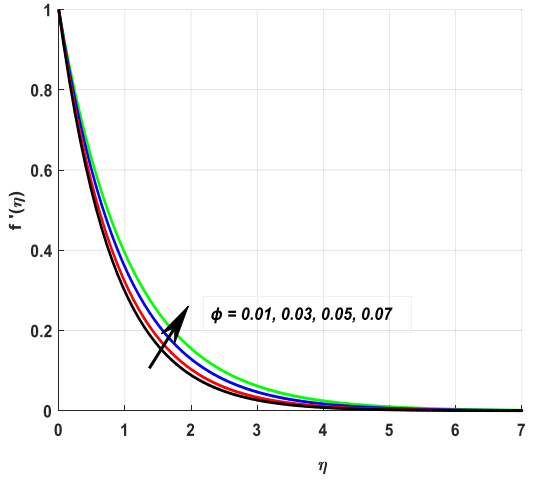

(d): Velocity attached with ϕ.

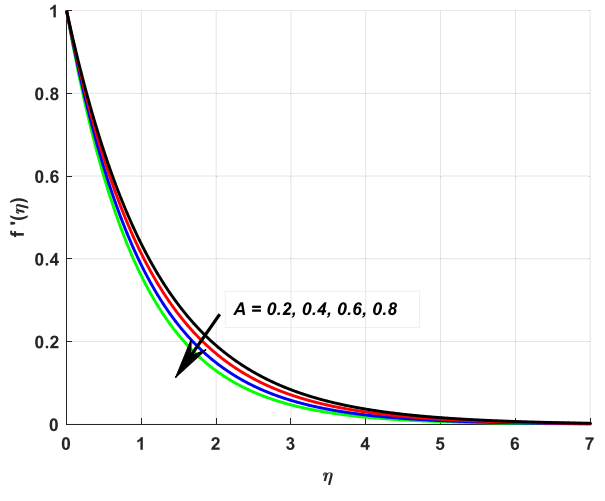

(e): Velocity attached with *A*.

(caption on next page)

Fig. 2. (a): Velocity attached with *We.* (b): Velocity attached with *n.* (c): Velocity attached with λ. (d): Velocity attached with ϕ. (e): Velocity attached with *A.*

4. Now block technique is processed and solution is obtained with absolute difference 10^{-6} in two consecutive iterations.

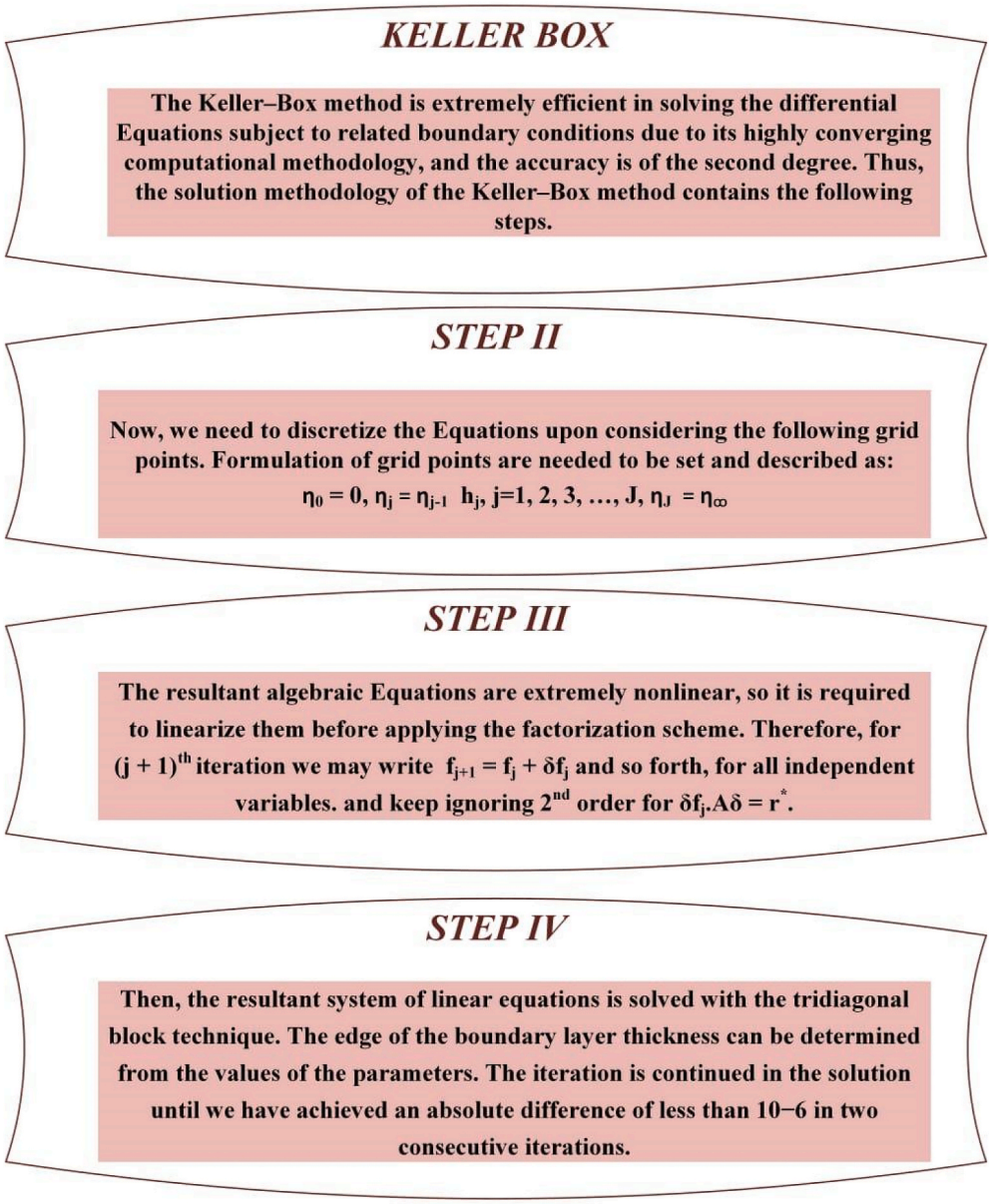

7. Results and discussions

This section attempts for revealing the impact of melting transport of energy and chemical species through autocatalysts on velocity, temperature, and profile of relocation of mass with taking mathematical model of Cross nanofluid (blood). Generated PDEs are converted into ODEs and passed through Bvp4c and KELLER BOX technique for getting its numerical results. Several parameters appeared in the system are checked with each profile. Detailed debated is launched here with each parameter like unsteadiness parameter ***A,*** Weissenberg number ***We,*** power law index ***n,*** Convection parameter ***λ,*** Prandtl number ***Pr,*** Schmidt number ***Sc,*** Melting

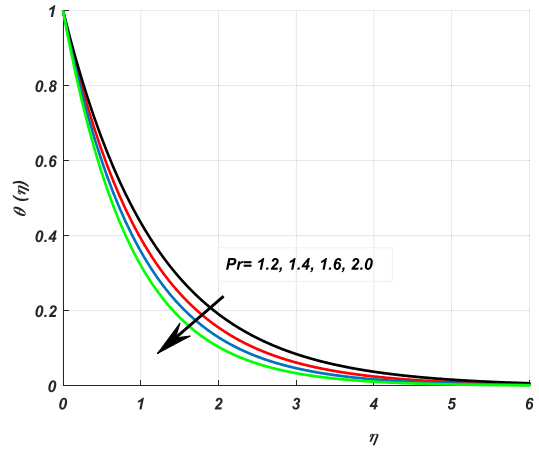

(a): Temperature attached with *Pr*.

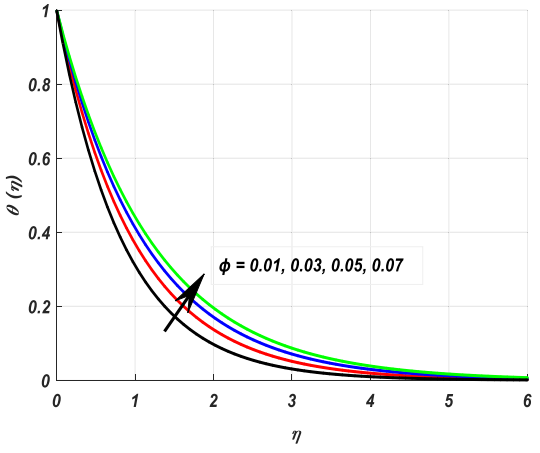

(b): Temperature attached with ϕ.

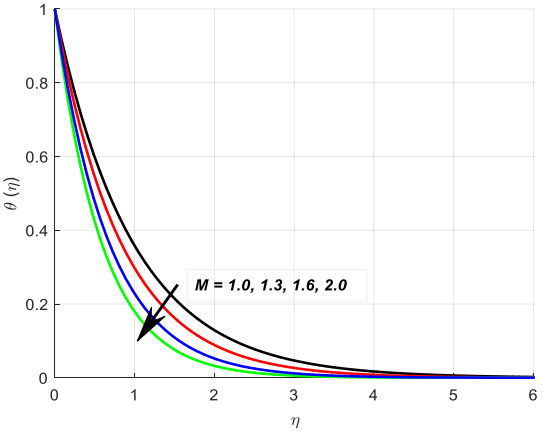

(c): Temperature attached with *M*.

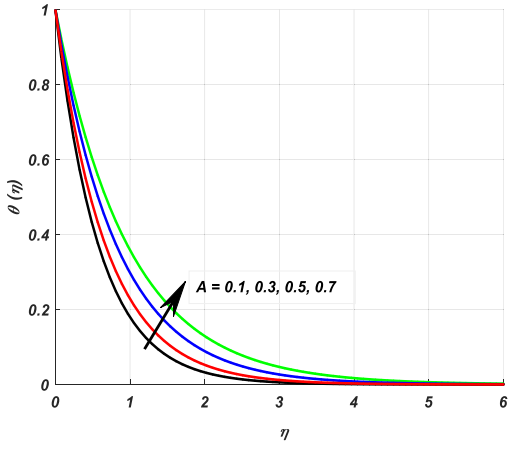

(d): Temperature attached with *A*.

Fig. 3. (a): Temperature attached with *Pr*. (b): Temperature attached with ϕ. (c): Temperature attached with *M*. (d): Temperature attached with *A*.

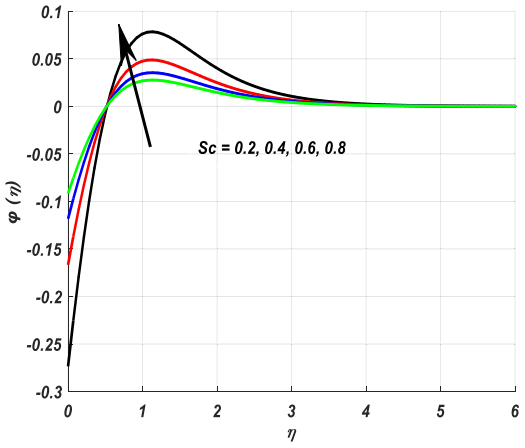

(a): Concentration attached with *Sc*.

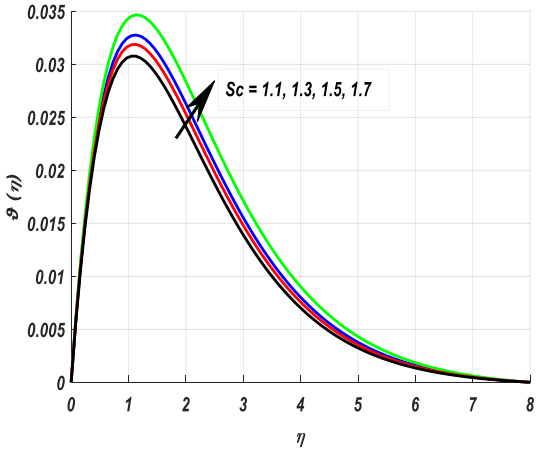

(b): Concentration attached with *Sc*.

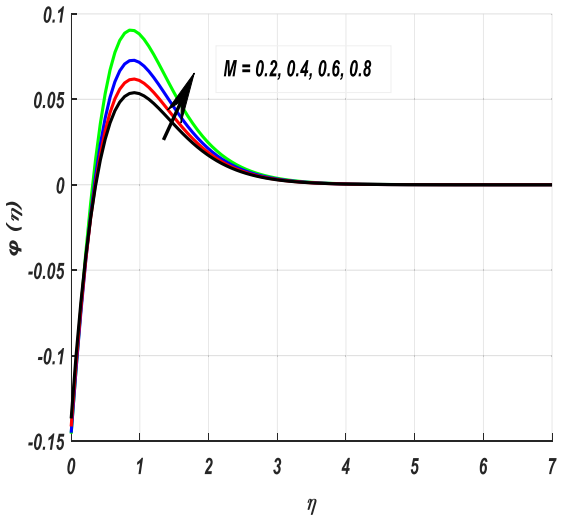

(c): Concentration attached with *M*.

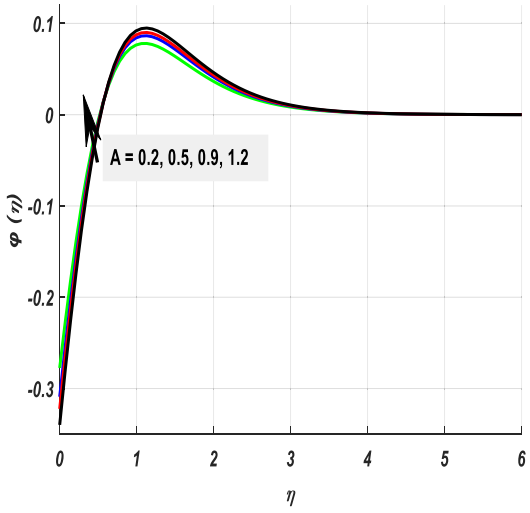

(d): Concentration attached with *A*.

Fig. 4. (a): Concentration attached with *Sc*. (b): Concentration attached with *Sc*. (c): Concentration attached with *M*. (d): Concentration attached with *A*. (e): Concentration attached with ϕ. (f): Concentration attached with ϕ. Concentration attached with k_2.

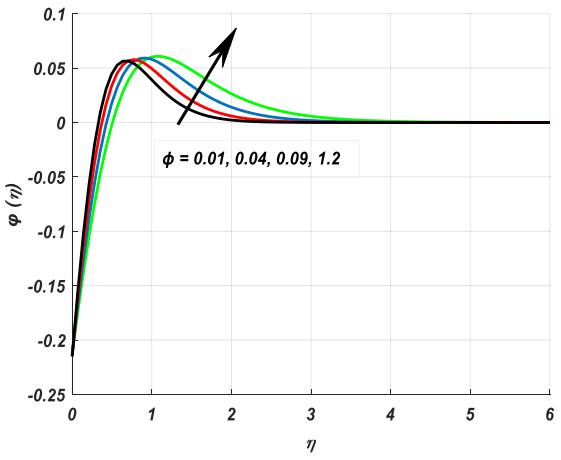

(e): Concentration attached with ϕ.

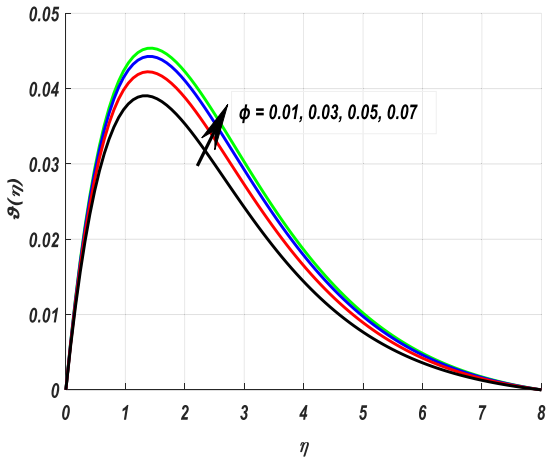

(f): Concentration attached with ϕ.

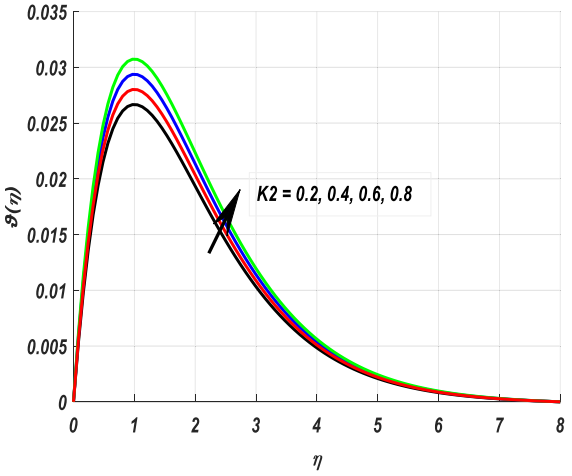

(g): Concentration attached with k_2.

Fig. 4. (*continued*).

parameter ***M,*** homogeneous reaction parameter k_2 and solid volume fraction of nanofluid $\boldsymbol{\phi}$ on each visibility. Discussion about physical quantities is also brought into consideration with effect of several parameter through tabular form. 3-D view of these quantities is also presented through smooth and clear statistical bar graphs.

Table 3 revels the impact of several variable on skin friction in case shear thinning/thickening case with comparison of two schemes bvp4c and Keller box. Similarly, Table 4 revels the impact of several variable on skin friction in case of opposing and assisting case with comparison of two schemes bvp4c and Keller box. Furthermore, Table 5 discusses the numerical interpretation of skin friction and Nusselt number with attached parameter with melting and without melting effect. Larger Melting parameter gives rapid transport of heat. Stronger values of φ gives greater magnitude of skin friction for both cases presence and absence of melting effect and rate of heat transport gets rapid in presence of melting effect and gets down in case of absence. Convection parameter makes increment in skin friction and rate of transport of energy in case of presence of melting process otherwise behave opposite. Stronger unsteadiness parameter and Prandtl number make increment in skin friction and Nusselt number for both cases of melting effect. For statistical analysis effect of all mentioned parameters with skin friction are sketched through Fig. 5(a–f), Fig. 6(a–h) and Fig. 7(a–f).

For geometrical interpretation of all present profiles there are figures (2-6) which describe the impact of several parameter on velocity, temperature and concentration of nanofluid (blood). Mathematically Weissenberg ***We*** is ratio of relaxation time and specific time and increment in it responds greater thickness of fluid due to this velocity of (blood) goes down. This fact is revealed out through Fig. 2 (a). Minifying value of Cross nanofluid (blood) index ***n*** *causes in reduction velocity visibility. Increasing value of* ***n*** *in the range* $0 < n$ goes in case of shear thickness so due to this reason velocity of nanofluid (blood) goes down and this is presented by Fig. 2 (b). Larger convection parameter responds lower velocity that is shown in Fig. 2 ***(c). For enlarge values of*** solid volume fraction of nanofluid (blood) $\boldsymbol{\phi}$ velocity of blood step-up due to volume fraction of nanofluid and this impact is shown by Fig. 2(d). Unsteadiness parameter ***A***

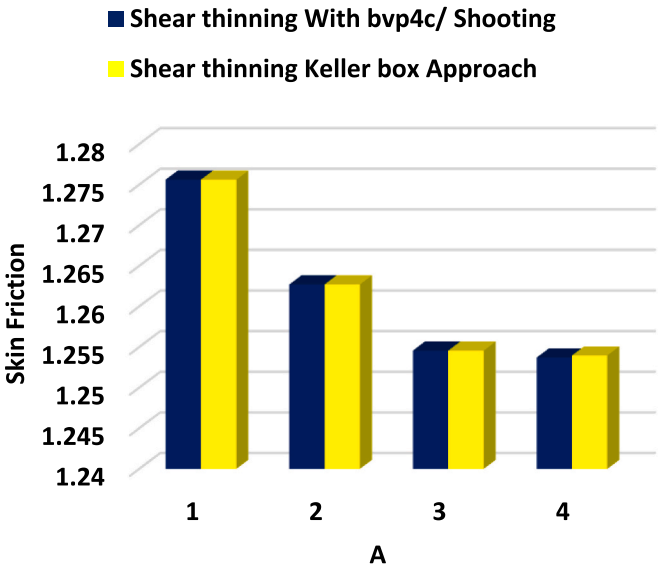

(a): Skin friction Concern with A

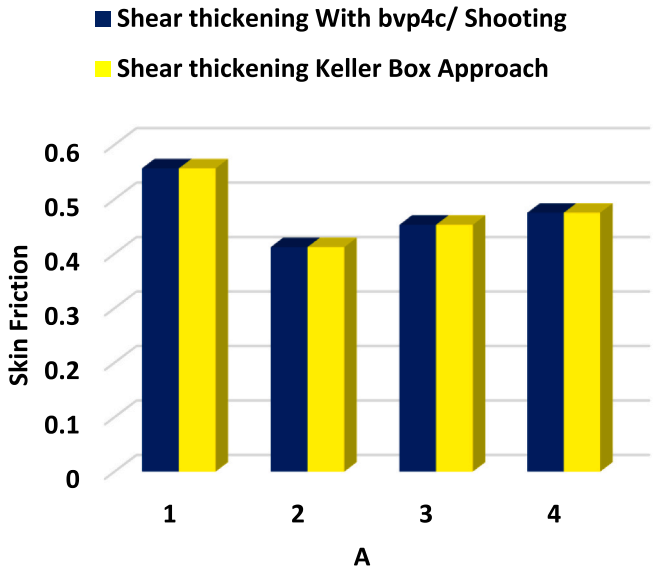

(b): Skin friction Concern with A

Fig. 5. (a): Skin friction Concern with A. (b): Skin friction Concern with A. (c): Skin friction Concern with ***We.*** (d): Skin friction Concern with ***We.*** (e): Skin friction Concern with ϕ. (f): Skin friction Concern with ϕ

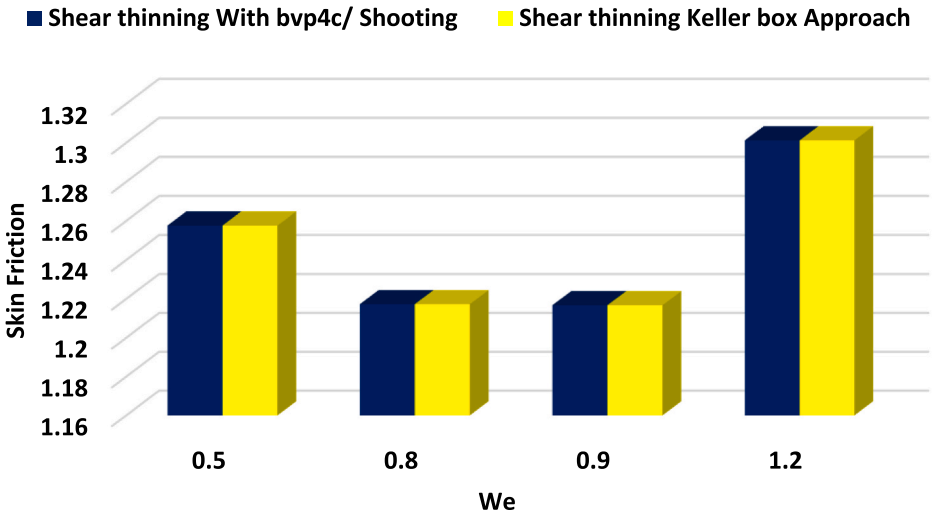

(c): Skin friction Concern with ***We***

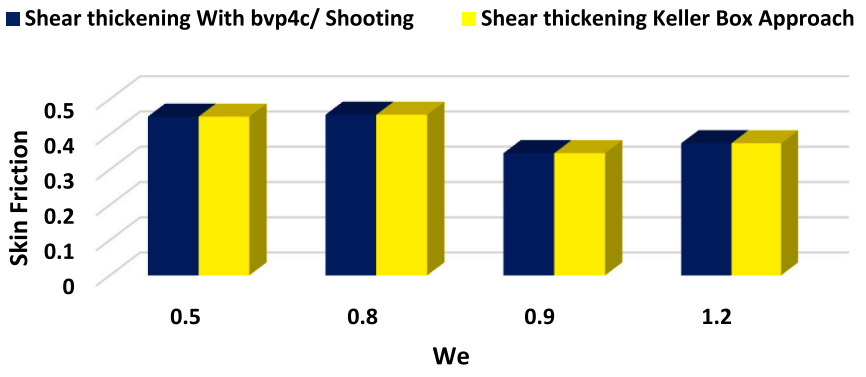

(d): Skin friction Concern with ***We***

Fig. 5. (*continued*).

is related with time factor so growth in this parameter results lower the velocity of nanofluid and unfolded by Fig. 2 (e). Plotting of temperature visibility along Prandtl number is sketched through Fig. 3(a). From this figure it is noticed that energy profile reduces with growing said parameter. This is reasoning that Pr corresponds lower boundary layer thickness due to this energy downs. ***For enlarge values of*** solid volume fraction of nanofluid (blood) ϕ temperature of blood step-up due to volume fraction of nanofluid. Melting process causes the enlarges the temperature and temperature profile for larger unsteadiness parameter gets downs due to time factor. These facts are shown with geometrical interpretation of Fig. 3(a), (b), 3(c), 3(d). Enhancement is encountered while growing to numerical values of Sc. Growth in Sc gives large rate of momentum diffusivity due to which larger Sc encourages the increment in Concentration of nanofluid (blood) and geometry of this fact can be seen through Fig. 4(a) and (b). Melting heat phenomenon also keeps its impact on profile of concentration and shown in Fig. 4 (c). It is noticed that growing the M the profile of concentration gets up due to melting process. Larger Unsteadiness parameter A gives greater concentration due to time factor. As velocity of nanofluid (blood) is getting low for greater unsteadiness parameter A, so during the low velocity transfer of mass can occur easily. This fact is described geometrically by Fig. 4 (d). Growing value of volume fraction of nanofluid parameter concentration grows due to greater temperature and shown in Fig. 4(e) and (f). Effect of homogeneous-heterogeneous parameter on concentration visibility is depicted by Fig. 4 (g) and it is noticed that growing value of said parameter the transport of mass gets up. When chemical process occurs, movement of nanoparticles are dispersed, and transport of mass become stronger.

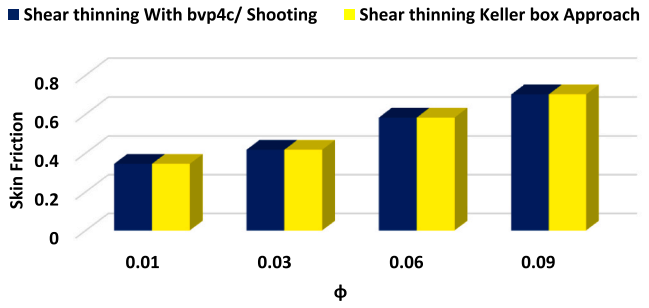

(e): Skin friction Concern with ϕ

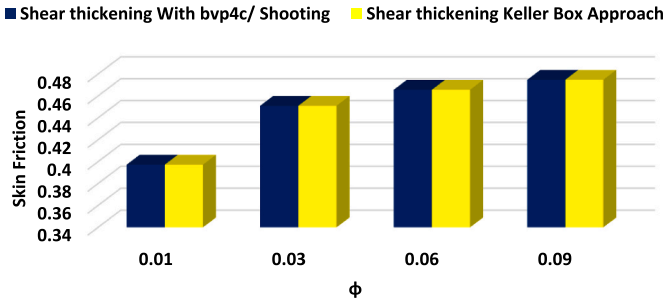

(f): Skin friction Concern with ϕ

Fig. 5. (*continued*).

6. Main points deduced by conclusion

This study unfolded the transport of blood energy containing nanoparticles of iron oxide (Fe_3O_4) and mass transport through homogeneous-heterogeneous chemical process with attached mathematical model of Cross fluid. Numerical outcome is done by two schemes named as two schemes i.e., bvp4c and Keller-box.

Few concluding remarks of this study are mentioned as:

1. It is noticed that mass transport is increased with greater homogeneous-heterogeneous chemical parameter.
2. Nanoparticles in fluid boosts the heat transfer.
3. Melting process causes to increase the transport of heat and skin friction.
4. Both schemes are compared and found smooth agreements.
5. Growth in solid volume fraction of nanofluid (blood) ϕ velocity of blood becomes greater.
6. Growth in Unsteadiness parameter A results lower the velocity of nanofluid.
7. Energy profile reduces with growing Pr parameter.

CRediT authorship contribution statement

Syed Zahir Hussain Shah: Conceptualization. **Assad Ayub:** Data curation. **Zulqurnain Sabir:** Formal analysis, Writing – original draft. **Waleed Adel:** Investigation. **Nehad Ali Shah:** Resources, Writing – review & editing. **Se-Jin Yook:** Supervision.

Declaration of competing interest

The authors declare that they have no known competing financial interests or personal relationships that could have appeared to influence the work reported in this paper.

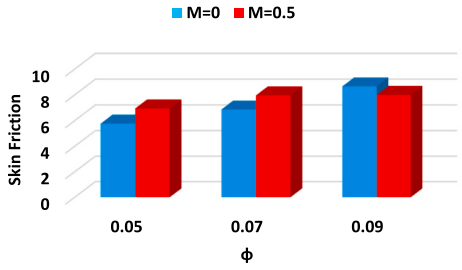

(a): Skin friction Concern with ϕ with and without melting process.

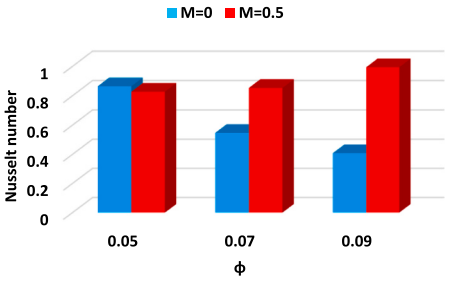

(b): Nusselt number Concern with ϕ with and without melting process.

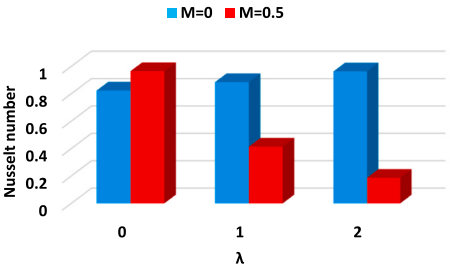

(c): Nusselt number Concern with l with and without melting process.

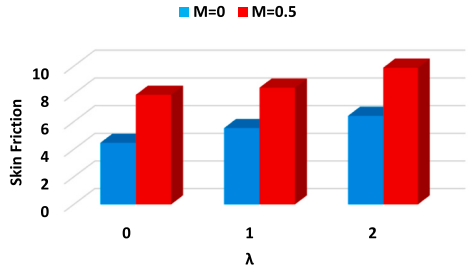

(d): Skin friction Concern with l with/without melting process.

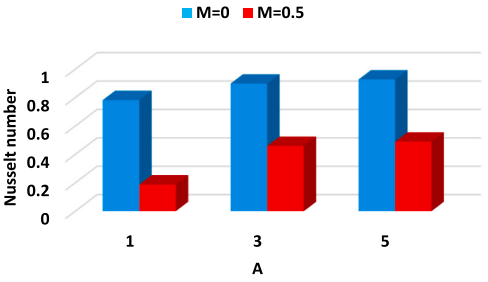

(e): Nusselt number Concern with A with/without melting process.

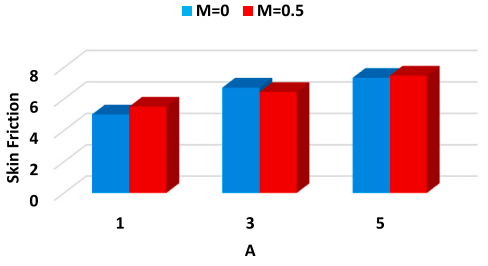

(f): Skin friction Concern with A with/without melting process.

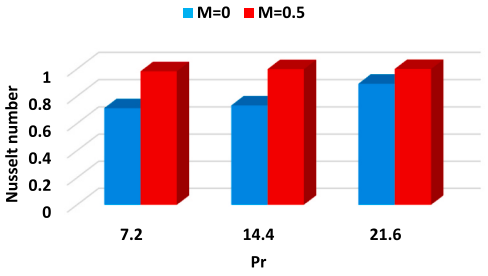

(g): Nusselt number Concern with Pr with/without melting process.

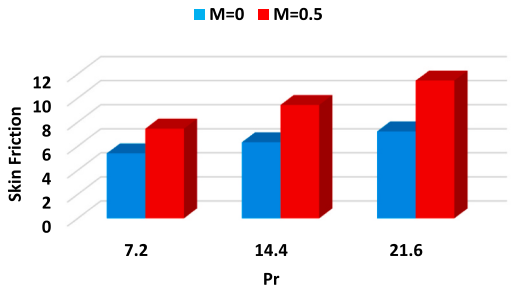

(h): Skin friction Concern with Pr with/without melting process.

Fig. 6. (a): Skin friction Concern with ϕ with and without melting process. (b): Nusselt number Concern with ϕ with and without melting process. (c): Nusselt number Concern with λ with and without melting process. (d): Skin friction Concern with λ with/without melting process. (e): Nusselt number Concern with A with/without melting process. (f): Skin friction Concern with A with/without melting process. (g): Nusselt number Concern with Pr with/without melting process. (h): Skin friction Concern with Pr with/without melting process.

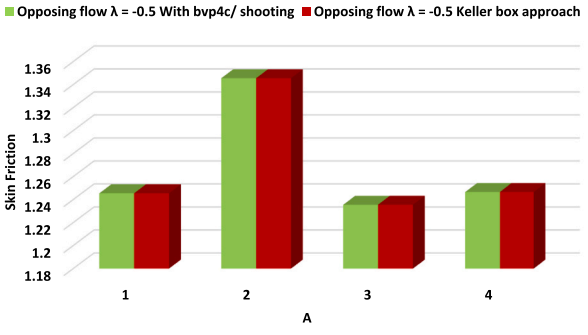

(a): Skin friction Concern with A with assisting and opposing flow

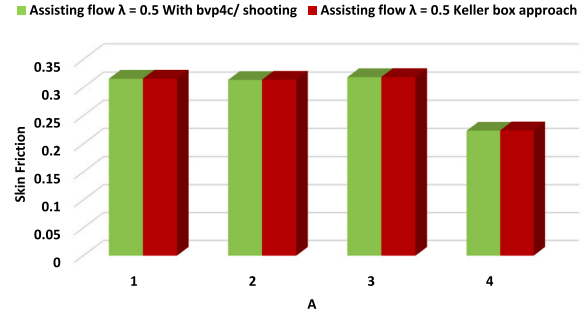

(b): Skin friction Concern with A with assisting and opposing flow.

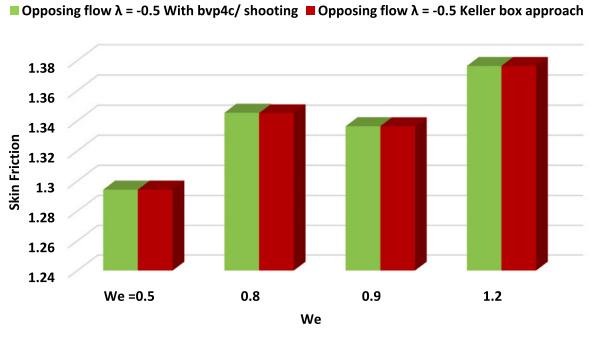

(c): Skin friction Concern with We with assisting and opposing flow.

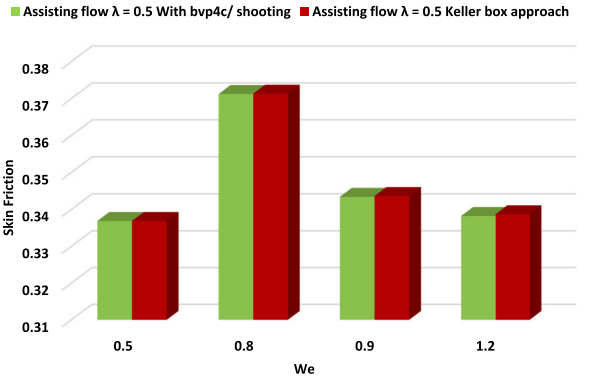

(d): Skin friction Concern with We with assisting and opposing flow.

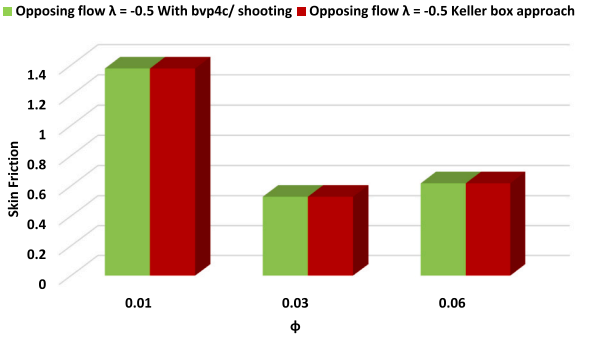

(e): Skin friction Concern with ϕ with assisting and opposing flow.

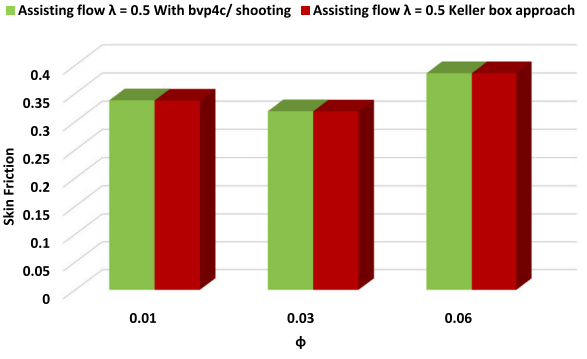

(f): Skin friction Concern with ϕ with assisting and opposing flow.

Figure 7. (a): Skin friction Concern with A with assisting and opposing flow. (b): Skin friction Concern with A with assisting and opposing flow. (c): Skin friction Concern with We with assisting and opposing flow. (d): Skin friction Concern with We with assisting and opposing flow. (e): Skin friction Concern with ϕ with assisting and opposing flow. (f): Skin friction Concern with ϕ with assisting and opposing flow.

Acknowledgments

The work in this paper has been supported by Basic Science Research Program through the National Research Foundation of Korea (NRF) funded by the Ministry of Science, ICT & Future Planning (Grant number: 2017R1A2B2006927).

References

[1] A. Mahammedi, H. Ameur, Y. Menni, D.M. Medjahed, Numerical study of turbulent flows and convective heat transfer of Al2O3-water nanofluids in A circular tube, J. Adv. Res. Fluid Mech. Thermal Sci. 77 (2) (2021) 1–12.
[2] Z. Sabir, A. Ayub, J.L. Guirao, S. Bhatti, S.Z.H. Shah, The effects of activation energy and thermophoretic diffusion of nanoparticles on steady micropolar fluid along with Brownian motion, Adv. Mater. Sci. Eng. (2020).
[3] S.Z. Shah, H.A. Wahab, A. Ayub, Z. Sabir, A. Haider, S.L. Shah, Higher order chemical process with heat transport of magnetized cross nanofluid over wedge geometry, Heat Tran. (2020) 1–24.
[4] A. Ayub, H.A. Wahab, Z. Sabir, A. Arbi, A note on heat transport with aspect of magnetic dipole and higher order chemical process for steady micropolar fluid, in: Fluid-Structure Interaction, IntechOpen, 2020.
[5] H.A. Wahab, Hussain Shah, A. Ayub, Z. Sabir, M. Bilal, G.C. Altamirano, Multiple characteristics of three-dimensional radiative Cross fluid with velocity slip and inclined magnetic field over a stretching sheet, Heat Tran. 50 (4) (2021) 3325–3341.
[6] A. Ayub, H.A. Wahab, S.Z. Shah, S.L. Shah, A. Darvesh, A. Haider, Z. Sabir, Interpretation of infinite shear rate viscosity and a nonuniform heat sink/source on a 3D radiative cross nanofluid with buoyancy assisting/opposing flow, Heat Tran. 50 (5) (2021) 4192–4232.
[7] C. Umadevi, M. Dhange, T. Sudha, B. Haritha, Flow of blood mixed with copper nanoparticles in an inclined overlapping stenosed artery with magnetic field, in: Case Studies in Thermal Engineering, 2021, p. 100947.
[8] A. Moradi, D. Toghraie, A.H.M. Isfahani, A. Hosseinian, An experimental study on MWCNT–water nanofluids flow and heat transfer in double-pipe heat exchanger using porous media, J. Therm. Anal. Calorim. 137 (5) (2019) 1797–1807.
[9] H. Vaidya, C. Rajashekhar, K.V. Prasad, S.U. Khan, F. Mebarek-Oudina, A. Patil, P. Nagathan, Channel flow of MHD bingham fluid due to peristalsis with multiple chemical reactions: an application to blood flow through narrow arteries, SN Appl. Sci. 3 (2) (2021) 1–12.
[10] A.J. Chamkha, M.A. Ismael, Magnetic field effect on mixed convection in lid-driven trapezoidal cavities filled with a Cu–water nanofluid with an aiding or opposing side wall, J. Therm. Sci. Eng. Appl. 8 (3) (2016).
[11] F. Abbas, H.M. Ali, M. Shaban, M.M. Janjua, T.R. Shah, M.H. Doranehgard, F. Farukh, Towards convective heat transfer optimization in aluminum tube automotive radiators: potential assessment of novel Fe2O3-TiO2/water hybrid nanofluid, J. Taiwan Instit. Chem. Eng. (2021).
[12] S. Yao, J. Wang, X. Liu, The influence of wall properties on convective heat transfer in isothermal nanochannel, J. Mol. Liq. 324 (2021) 115100.
[13] M. Goodarzi, D. Toghraie, M. Reiszadeh, M. Afrand, Experimental evaluation of dynamic viscosity of ZnO–MWCNTs/engine oil hybrid nanolubricant based on changes in temperature and concentration, J. Therm. Anal. Calorim. 136 (2) (2019) 513–525.
[14] A. Shahsavar, S. Khanmohammadi, D. Toghraie, H. Salihepour, Experimental investigation and develop ANNs by introducing the suitable architectures and training algorithms supported by sensitivity analysis: measure thermal conductivity and viscosity for liquid paraffin based nanofluid containing Al2O3 nanoparticles, J. Mol. Liq. 276 (2019) 850–860.
[15] P. Barnoon, D. Toghraie, R.B. Dehkordi, H. Abed, MHD mixed convection and entropy generation in a lid-driven cavity with rotating cylinders filled by a nanofluid using two phase mixture model, J. Magn. Magn Mater. 483 (2019) 224–248.
[16] S.U. Choi, J.A. Eastman, *Enhancing Thermal Conductivity of Fluids with Nanoparticles* (No. ANL/MSD/CP-84938; CONF-951135-29), Argonne National Lab., IL (United States), 1995.
[17] R. Ellahi, S.U. Rahman, S. Nadeem, N.S. Akbar, Blood flow of nanofluid through an artery with composite stenosis and permeable walls, Appl. Nanosci. 4 (8) (2014) 919–926.
[18] M.M. Rashidi, M.M. Bhatti, M.A. Abbas, M.E.S. Ali, Entropy generation on MHD blood flow of nanofluid due to peristaltic waves, Entropy 18 (4) (2016) 117.
[19] H.S. Chahregh, S. Dinarvand, TiO2-Ag/blood hybrid nanofluid flow through an artery with applications of drug delivery and blood circulation in the respiratory system, Int. J. Numer. Methods Heat Fluid Flow (2020).
[20] J. Tripathi, B. Vasu, O.A. Bég, Computational simulations of hybrid mediated nano-hemodynamics (Ag-Au/Blood) through an irregular symmetric stenosis, Comput. Biol. Med. 130 (2021) 104213.
[21] D. Toghraie, M. Mahmoudi, O.A. Akbari, F. Pourfattah, M. Heydari, The effect of using water/CuO nanofluid and L-shaped porous ribs on the performance evaluation criterion of microchannels, J. Therm. Anal. Calorim. 135 (1) (2019) 145–159.
[22] M.M. Cross, Rheology of non-Newtonian fluids: a new flow equation for pseudoplastic systems, J. Colloid Sci. 20 (5) (1965) 417–437.
[23] R. Ponalagusamy, R.T. Selvi, A.K. Banerjee, Mathematical model of pulsatile flow of non-Newtonian fluid in tubes of varying cross-sections and its implications to blood flow, J. Franklin Inst. 349 (5) (2012) 1681–1698.
[24] A.R. Haghighi, N. Pirhadi, M. Shahbazi Asl, A Mathematical modeling for the study of blood flow as a cross fluid through a tapered artery, J. New Res. Math. 5 (20) (2019) 15–30.
[25] M. Nazeer, Numerical and perturbation solutions of cross flow of an Eyring-Powell fluid, SN Appl. Sci. 3 (2) (2021) 1–11.
[26] Z. Sabir, A. Imran, M. Umar, M. Zeb, M. Shoaib, M.A.Z. Raja, A numerical approach for two-dimensional Sutterby fluid flow bounded at a stagnation point with an inclined magnetic field and thermal radiation impacts, Therm. Sci. (2020) 186, 186.
[27] M.I. Khan, T. Hayat, M.I. Khan, A. Alsaedi, Activation energy impact in nonlinear radiative stagnation point flow of Cross nanofluid, Int. Commun. Heat Mass Tran. 91 (2018) 216–224.
[28] L. Yao, A. Grishaev, G. Cornilescu, A. Bax, The impact of hydrogen bonding on amide 1H chemical shift anisotropy studied by cross-correlated relaxation and liquid crystal NMR spectroscopy, J. Am. Chem. Soc. 132 (31) (2010) 10866–10875.
[29] R.P. Sharma, S.R. Mishra, Effect of higher order chemical reaction on magnetohydrodynamic micropolar fluid flow with internal heat source, Int. J. Fluid Mech. Res. 47 (2) (2020).
[30] M.I. Khan, M. Waqas, T. Hayat, A. Alsaedi, A comparative study of Casson fluid with homogeneous-heterogeneous reactions, J. Colloid Interface Sci. 498 (2017) 85–90.
[31] M. Khan, L. Ahmad, M. Ayaz, Numerical simulation of unsteady 3D magneto-Sisko fluid flow with nonlinear thermal radiation and homogeneous–heterogeneous chemical reactions, Pramana 91 (1) (2018) 1–11.
[32] M. Irfan, M. Khan, W.A. Khan, Impact of homogeneous–heterogeneous reactions and non-Fourier heat flux theory in Oldroyd-B fluid with variable conductivity, J. Braz. Soc. Mech. Sci. Eng. 41 (3) (2019) 1–9.
[33] A. Mahdy, Impacts of homogeneous-heterogeneous chemical reactions and inclined magnetic field on unsteady nanofluids flow, AIP Adv. 8 (11) (2018) 115109.
[34] M. Waqas, A mathematical and computational framework for heat transfer analysis of ferromagnetic non-Newtonian liquid subjected to heterogeneous and homogeneous reactions, J. Magn. Magn Mater. 493 (2020) 165646.
[35] M.I. Khan, T. Hayat, M. Waqas, M.I. Khan, A. Alsaedi, Impact of heat generation/absorption and homogeneous-heterogeneous reactions on flow of Maxwell fluid, J. Mol. Liq. 233 (2017) 465–470.
[36] D. Toghraie, N.N. Esfahani, M. Zarringhalam, N. Shirani, S. Rostami, Blood flow analysis inside different arteries using non-Newtonian Sisko model for application in biomedical engineering, Comput. Methods Progr. Biomed. 190 (2020) 105338.
[37] M. Ijaz, M. Ayub, M.Y. Malik, H. Khan, A.A. Alderremy, S. Aly, Entropy analysis in nonlinearly convective flow of the Sisko model in the presence of Joule heating and activation energy: the Buongiorno model, Phys. Scripta 95 (2) (2020), 025402.

[38] K. Han, X. Zheng, B. Sun, G. He, R. Zhang, Chemical reaction dynamics of barium atom with alkyl bromides, Chem. Phys. Lett. 181 (5) (1991) 474–478.
[39] M.J. Zyphur, E.L. Hamaker, L. Tay, M. Voelkle, K.J. Preacher, Z. Zhang, E.F. Diener, From data to causes III: Bayesian priors for general cross-lagged panel models (GCLM), Front. Psychol. 12 (2021) 112.
[40] A.R. Gheynani, O.A. Akbari, M. Zarringhalam, G.A.S. Shabani, A.A. Alnaqi, M. Goodarzi, D. Toghraie, Investigating the effect of nanoparticles diameter on turbulent flow and heat transfer properties of non-Newtonian carboxymethyl cellulose/CuO fluid in a microtube, Int. J. Numer. Methods Heat Fluid Flow (2019).
[41] H. Arasteh, R. Mashayekhi, D. Toghraie, A. Karimipour, M. Bahiraei, A. Rahbari, Optimal arrangements of a heat sink partially filled with multilayered porous media employing hybrid nanofluid, J. Therm. Anal. Calorim. 137 (3) (2019) 1045–1058.
[42] S. Gupta, K. Sharma, Numerical simulation for magnetohydrodynamic three dimensional flow of Casson nanofluid with convective boundary conditions and thermal radiation, Eng. Comput. (2017).
[43] S. Gupta, K. Sharma, Numerical simulation for magnetohydrodynamic three dimensional flow of Casson nanofluid with convective boundary conditions and thermal radiation, Eng. Comput. (2017).
[44] L.J. Grubka, K.M. Bobba, Heat transfer characteristics of a continuous stretching surface with variable temperature, ASME J. Heat Tran. 107 (1) (1985) 248–250.
[45] M.S. Abel, N. Mahesha, Heat transfer in MHD viscoelastic fluid flow over a stretching sheet with variable thermal conductivity, non-uniform heat source and radiation, Appl. Math. Model. 32 (10) (2008) 1965–1983.
[46] M. Umar, R. Akhtar, Z. Sabir, H.A. Wahab, Z. Zhiyu, A. Imran, M.A.Z. Raja, Numerical treatment for the three-dimensional eyring-powell fluid flow over a stretching sheet with velocity slip and activation energy, Adv. Math. Phys. (2019). *2019*.
[47] Z. Sabir, R. Akhtar, Z. Zhiyu, M. Umar, A. Imran, H.A. Wahab, M.A.Z. Raja, A computational analysis of two-phase casson nanofluid passing a stretching sheet using chemical reactions and gyrotactic microorganisms, Math. Probl Eng. (2019).
[48] M. Umar, Z. Sabir, A. Imran, A.H. Wahab, M. Shoaib, M.A.Z. Raja, The 3-D flow of Casson nanofluid over a stretched sheet with chemical reactions, velocity slip, thermal radiation and Brownian motion, Therm. Sci. 24 (5 Part A) (2020) 2929–2939.
[49] T. Sajid, S. Tanveer, Z. Sabir, J.L.G. Guirao, Impact of activation energy and temperature-dependent heat source/sink on maxwell–sutterby fluid, Math. Probl Eng. (2020).
[50] Z. Sabir, A. Imran, M. Umar, M. Zeb, M. Shoaib, M.A.Z. Raja, A numerical approach for two-dimensional Sutterby fluid flow bounded at a stagnation point with an inclined magnetic field and thermal radiation impacts, 00, Therm. Sci. (2020) 186, 186.
[51] Z. Sabir, M.A.Z. Raja, C.M. Khalique, C. Unlu, Neuro-evolution computing for nonlinear multi-singular system of third order Emden–Fowler equation, Math. Comput. Simulat. 185 (2021) 799–812.
[52] Z. Sabir, M.G. Sakar, M. Yeskindirova, O. Saldir, Numerical investigations to design a novel model based on the fifth order system of Emden–Fowler equations, Theor. Appl. Mech. Lett. 10 (5) (2020) 333–342.
[53] A. Ayub, H.A. Wahab, S.Z. Hussain Shah, S.L. Shah, Z. Sabir, S. Bhatti, On heated surface transport of heat bearing thermal radiation and MHD Cross flow with effects of nonuniform heat sink/source and buoyancy opposing/assisting flow, Heat Transfer (2021) 1–19, https://doi.org/10.1002/htj.22164.
[54] A. Ayub, A. Darvesh, G.C. Altamirano, Z. Sabir, Nanoscale energy transport of inclined magnetized 3D hybrid nanofluid with Lobatto IIIA scheme, Heat Tran. (2021), https://doi.org/10.1002/htj.22188.
[55] A. Ayub, Z. Sabir, G.C. Altamirano, et al., Characteristics of melting heat transport of blood with time-dependent cross-nanofluid model using Keller–Box and BVP4C method, Eng. Comput. (2021), https://doi.org/10.1007/s00366-021-01406-7.